Low Power Consumption Design of Micro-machined Thermal Sensor for Portable Spirometer

Nan-Fu Chiu[1], Tzu-Chien Hsiao[3,4] and Chii-Wann Lin[1,2]*

[1]*Institute of Electrical Engineering, National Taiwan University*
Taipei, Taiwan 106, R.O.C.
[2]*Institute of Biomedical Engineering, National Taiwan University*
Taipei, Taiwan 106, R.O.C.
[3]*Biomedical Research & Development, Hsinchin Biomedical Science Park*
National Taiwan University
Taipei, Taiwan 106, R.O.C.
[4]*Department of Biomedical Engineering, I-Shou University*
Taiwan 840, R.O.C.

Abstract

There are great needs for a low cost and low power consumption portable spirometer for the home care of respiratory diseases. Thermal anemometer has the advantage of possible miniaturization by modern microfabrication processes. However, its optimal design remains to be a technical challenge for the trade off between required sensitivity and power consumption. The designed features of such a sensor include low thermal conduction via substrate, wide dynamic range (0~180 L/Min) to cover high peak flow rate and possible low cost mass production. To meet these requirements, we used both surface and bulk micromachining techniques to fabricate the sensor for optimal performance. Testing of constructed prototype showed that it can be used under low operating voltage of 3 volts. According to the American Thoracic Society (ATS) guidance for the measurement of pulmonary functions, including dynamic volume of forced expiratory vital capacity (FVC) and flow during forced expiration: peak expiratory flow rate (PEFR), it has necessary accuracy (≤ 3% variation) for diagnosis requirements.

Key Words: Thermal Anemometeric Chip, Portable Spirometer, ATS, FVC, PEFR

1. Introduction

In the United States, there are estimated 16 million adults with chronic obstructive pulmonary diseases (COPDs) and another 17 million suffer from asthma and children account for 4.8 million of the group. Although asthma deaths are infrequent, it has increased significantly during the last two decades. It claims more than 5,000 lives due to asthma alone each year in the United States [1,2]. The measurement of static and dynamic respiratory functions provides important indexes for diagnosis of asthma and COPD. A spirometer can measure the flow or volume of gas moving into and out of the lungs during inspiratory and expiratory cycles. It becomes a need for home-care personalized devices due to the increasing number of respiratory related diseases. The efforts to provide a portable, user-friendly and accurate electronic spirometer have resulted in many new developments in both flow sensors and systems [3,4]. In the past, we have reported a simple flow sensor of 1.2 kΩ impedance, which required higher operating voltage (~10 V) to get stable output signal. It was found that the sensor temperature is around 120 °C [5,6]. It thus requires new design and fabrication processes to meet the low power consumption requirement. In this paper, we report the development of a micro-machined thermal anemometer and a portable microsystem for home care uses. The testing results of the constructed prototype according to the guidelines of related recommendations and standards are also discussed.

*Corresponding author. E-mail: cwlinx@ntu.edu.tw

2. Materials and Methods

A lot of current respiratory indexes are based on the measurement of volume, e.g. tidal volume, inspiratory/expiratory volume, and dead space volume. It is rather difficult to miniaturize this type of instrument. Alternatively, one can measure flow rate with known orifice geometry and then do the time integral to get the total volume, which opens up possible technology innovations for mininaturization. One of the available operating principles for flow measurement is thermal anemometry [7,8]. It measures the total heat loss of a heating element and correlates the output signal to the flow rate of the fluid. It normally operates in one of three modes: constant current, constant temperature, or constant power. With the available micro-machined techniques, performance/cost ratio can be further enhanced with possible standard mass production and on board CMOS circuitry for nonlinear compensation [9,10].

2.1 Principle of Thermal Anemometers

Heat loss or gain can occur through an element of the building sensor by three primary mechanisms: 1) conduction, 2) convection, 3) radiation. In heat transfer sensors, a known temperature difference, is maintained between the hot part and cold part of the sensor. This thermal energy will transfer to the cold part by means of the following paths with losses rate, i.e., natural convection rate (Q'_{NC}), forced convection rate (Q'_{FC}), thermal conduction rate (Q'_{C}) and thermal radiation losses rate (Q'_{R}). The total heating power p during thermal equilibrium should be equal to the summation of possible heat dissipation pathways as shown in the Figure 1 and expressed as in the following equation.

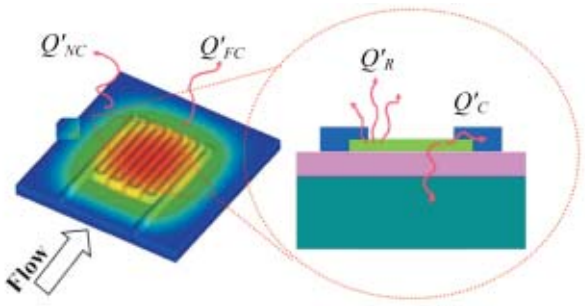

Figure1. Schematic diagram of a micro-machined thermal anemometry sensor shows four common heat transfer paths and losses rate of natural and forced convection (Q'_{NC}, Q'_{FC}), radiation (Q'_{R}) and conduction (Q'_{C}).

$$P_{heating-power} = Q'_{R} + Q'_{NC} + Q'_{C} + Q'_{FC} \quad (1)$$

It must be noted that when the structure is small enough, radiation and natural convection losses are negligible for most of the operating conditions. However, the conduction and forced convection heat loss can be large, so that Eq. (1) can be reduced and expressed as Eq. (2), where G_{air} and G_{si} denote geometry factors of the heat transfer pathways through the air and the substrate membrane, and λ_{air} and λ_{si} denote the thermal conductivity of the air and substrate membrane, respectively. To optimize the sensor performance for higher sensitivity and lower power consumption, one can maximize Q'_{FC} for better sensitivity and minimize Q'_{C} for lower power consumption [4,11,12].

$$P_{heating-power} = Q'_{FC} + Q'_{C} = G_{air}\lambda_{air}\Delta T + G_{Si}\lambda_{Si}\Delta T \quad (2)$$

$$Q'_{FC} = S \cdot (T_S - T_a) \quad (3)$$

$$Q'_{C} = k \cdot S \cdot (\frac{dT}{dx}) \quad (4)$$

In the Eqs. (3) and (4), for a one dimensional, steady state heat flow the dissipitation rate is expressed by Fourier's equation, where S is contact area, T_s is sensor temperature, T_a is ambient temperature, k is thermal conductivity (W/m-k), which describes the material's ability to conduct heat; x is distance of heat flow, and dT is temperature difference.

Due to the heterogeneous nature of typical MEMS hot-plate chip, which typically employing glass or silicon substrate and metallic thin films, the thermal conductivity depends on the relative thickness of each individual layer and its orientation with respect to heat flow. We can define thermal impedance, R_θ, as shown in Eq. (5) for non-homogeneous structure. These two parameters, i.e., thermal conductivity and thermal impedance, describe heat transfer within a material. The relationship between k and R_θ is shown as in the Eq. (6).

$$R_\theta = S\frac{\Delta T}{Q'_{C}} \quad (5)$$

$$k = \frac{x}{R_\theta}, \quad R_\theta = R_{material} + R_{contact} \quad (6)$$

The thermal impedance, R_θ, of a material is defined as the summation of its thermal resistance and contact resistance. The contact resistance would thus include the

effects of surface roughness, clamping pressure, material thickness and compressive modulus.

The principle of the thermal anemometer can be described by the following equations with power (7) delivered to the sensor.

$$P = I^2 R_S = hS(T_S - T_f) \tag{7}$$

$$h = C_0 + C_1 v^n \tag{8}$$

$$R_S = R_0 e^{B\left(\frac{1}{T_S}-\frac{1}{T_0}\right)} = Ae^{\frac{B}{T_S}} \tag{9}$$

$$\frac{R_S(T_S)}{R_S(T_0)} = 1 + \alpha_{T_0}(T_S - T_0) \tag{10}$$

$$\begin{aligned}\alpha_{T_0} &= \frac{1}{R_s(T_0)}\frac{R_S(T_S)-R_S(T_0)}{(T_S-T_0)} \\ &= \frac{1}{R_S(T_0)}\frac{dR_S(T_S)}{dT_S}\end{aligned} \tag{11}$$

$$T_S = \frac{1}{\alpha_{ref}}\frac{R(T_S)-R(T_{ref})}{R(T_{ref})} + T_{ref} = \frac{a}{\alpha_{ref}} + T_{ref} \tag{12}$$

$$T_{ref} = \frac{T_S + T_f}{2} \tag{13}$$

$$\begin{aligned}E_{out}(T_{ref}) &= E_{out}(T)\sqrt{\frac{T_S - T_{ref}}{T_S - T}} \\ &= E_{out}(T)\sqrt{\frac{R(T_S)-R(T_{ref})}{R(T_S)-R(T)}}\end{aligned} \tag{14}$$

Where: $A = R_0 e^{-\frac{B}{T_0}}$

P = resistance of the hot-plate sensor at temperature T_S;
h = heat transfer coefficient referred to the sensor surface in W/m^{2}K;
S = wL surface area of the sensor (w = width, L = length)
ν = the fluid velocity, and C_0 and C_1 are experimental constants;
B = material dependent temperature constant
T_s = temperature of the hot-plate sensor at work (K);
R_s = hot-plate sensor resistance at temperature T_S;
R_0 = resistance at temperature T_0;
T_0 = reference temperature (K);
T_f = fluid temperature (K);
T_{ref} = calibrate hot-plate sensor reference temperature (K);
α_{T_0} = resistance temperature coefficient at T_0;
α_{ref} = hot-plate sensor reference temperature (K) temperature coefficient;

In (8) h depends on the fluid mass flux (ρ* Q) and dimension of sensor. The function between h and velocity can be experimentally determined by best fitting the parameters in the first order approximation of the modified King's law for free convection heat transfer at low Reynolds number (R_e) in a long cylindrical structure [13–15]. The common method of measuring the resistance change of a hot-plate sensor is to build the probe into an arm of a Wheatstone-bridge circuits, the hot-plate sensor output voltage is Eq. (14).

2.2 Design of Micro-machined Thermal Flow Sensor

One of the important design issues is the operating temperature of the sensor comparing to normal body temperature, especially for low power consumption. To optimize sensor performance, the designed sensor has to decrease its resistance and heat capacity but increase surface area for sensing of flow. The optimal range of resistance should be in the range of 35~500 Ω. The optimal working temperature of the sensor would be around 70 °C with current of 1~15 mA [6].

From above mentioned criterions, there are some important issues that we have to consider as well. These include material thermal conductivity, sensitivity, flow direction, and structure. Figure 2 shows two different structure designs of thermal sensor, ie. thin film resistor on a) bulk silicon and b) Si_3N_4 by back etching. We used the FLOTHERM® software to simulate and compare their performance in theoretical settings.

2.3 Fabrication Process

Typical metallic thin film deposition and patterning

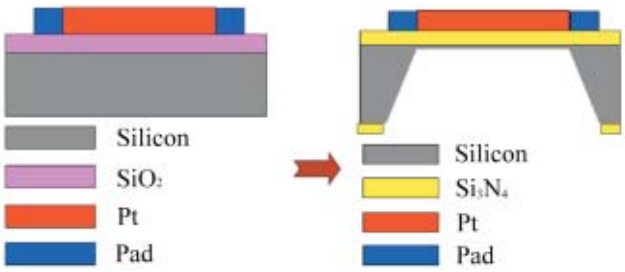

Figure 2. Two different designs of Pt thin film thermal anemometer based on a) Bulk silicon and b) back etching structure.

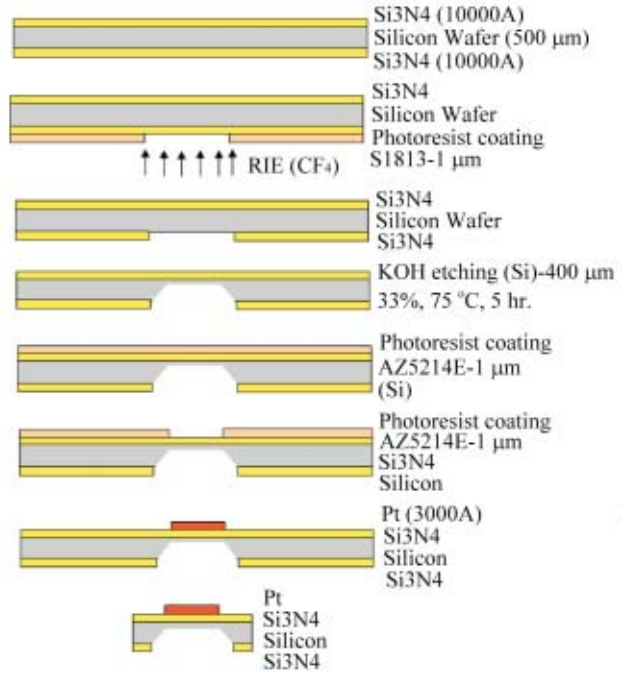

Figure 3. Microfabrication processes flow for thermal anemometry sensor with back etching on Si3N4 membrane.

processes are used in microfabrication of proposed sensors. N-type 4 inch, 500 μm thick, silicone wafer <100> after routine cleaning procedures was put into PECVD oven to grow Si3N4 (10000 Å) on both sides. After lithography patterning, the Si3N4 was opened by RIE etched, and then backside etched in 33% KOH solution at 75 °C to form pyramidal pits. The front side was patterned by lithography and deposited 3000 Å Pt heating layers by an E-beam evaporator over the Si3N4 and patterned by lift off process. Figure 3 shows the fabrication processes.

2.4 Testing Apparatus

Functional tests and verifications of fabricated microsensors and prototype are conducted by using a reference standard of 3 liter syringe (A-M systems Inc., USA) for volume sensing and a flow calibration analyzer (RT-200, Allied Healthcare Inc., USA) for flow sensing. A home-made environmental box is used to contol the inlet gas flow rate, temperature and humidity that flows through the connected device under test.

3. Results and Discussion

3.1 Simulation of Structure Design

The thermal conduction through substrate contact is the major heat loss without back etching through silicone wafer. Figure 4 shows the simulation results of two different structures: a) flat contact and b) back etching. In the first case, the temperature of the substrate follows thin film heat source very closely, which is less optimal for the flow sensor uses. In the later case, the temperature of the thin film source does not propagate into substrate due to the presence of air gap. It makes most of the generated heat dissipate through air convection instead of substrate conduction.

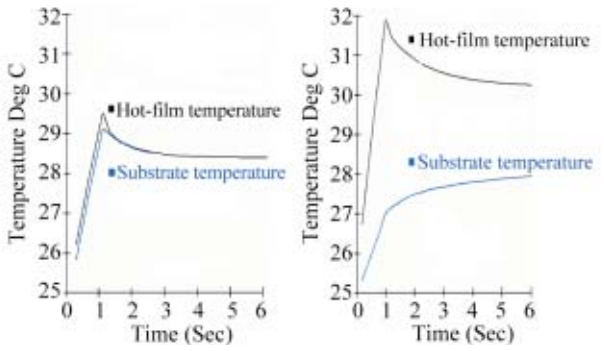

Figure 4. Thermal conduction simulation results of a) flat contact sensor structure and b) back etching structure in the air flow. In the first case, a lot of heat dissipates through substrate. The temperature of substrate follows hot-film closely. In the later case, most of the generated heat is radiated through air instead of substrate. So the temperature profiles of these two elements deviate from each other.

3.2 Fabricated Sensor and Performance

Following previous mentioned fabrication processes, Figure 5 shows one of the fabricated thermal anemome-

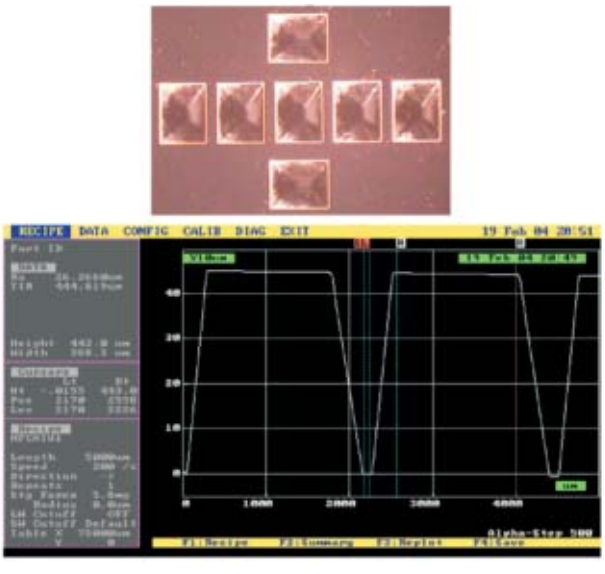

Figure 5. Experimental results for thickness of an etched.

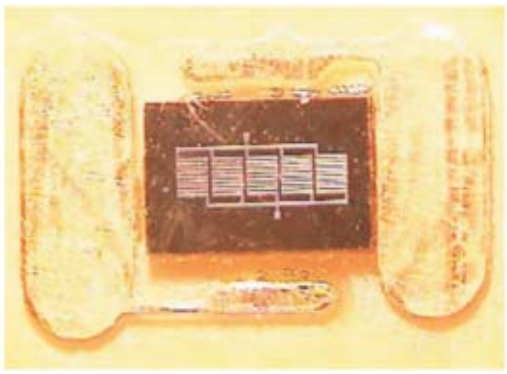

Figure 6. Assembled thin film thermal anemometer sensor with wire bonded on a printed circuit board to testing.

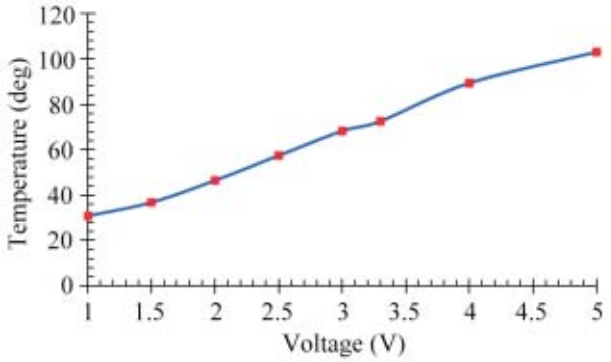

Figure 7. Temperature measurements of assembled thermal anemometry sensor under different operating bias from 1 to 5 volt., it is about 68 degree with 3 volt.

ter chips. The chip size is about 2 mm*2 mm*0.5 mm. Its geometrical features of sensing site, which is 443 um in thickness and 388 μm width by using a standard surface profiler. The sensor element, as shown in the Figure 6, was used in the following functional studies. Its power consumption under constant voltage of 3 V in air is about 39.8 mW. Figure 7 shows the temperature measurement results of this sensor under different operating voltage.

The validation of the designed sensor by using a thermal imager can be used for the measurement of input different voltage on hot-plate sensor surface temperature profile. Figure 7 shows the resultant thermal and input voltage relation. The sensor element reaches 72.5 °C with constant voltage of 3.3 V in this case, which is in our design specification.

3.3 Spirometer System

A potable pocket sized spirometric system is constructed and shown in Figure 8, in which the described thermal anemometric sensor is positioned in the center of the open tube. This prototype is then put into a testing chamber with temperature and humidity control. We used high pressure air source with variable control valve to have different flow velocity the construct a calibration curve for the spirometric system. The reading on the calibration analyzer is recorded and plot against the Vout

Figure 8. Prototype of a portable pocket-sized spirometer, in which the described micro-machined thermal anemometer has been implemented and assembled for functional testing is shown in the photo with a ten dollor coin.

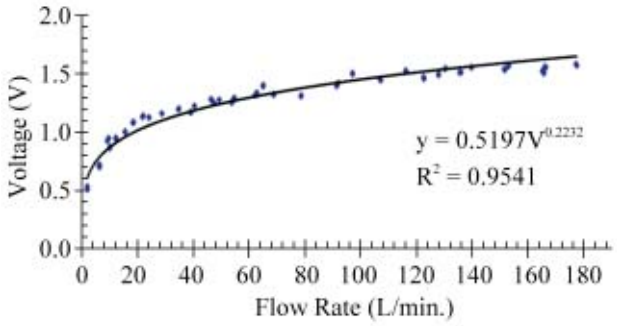

Figure 9. The calibration cure of thermal anemometer placed in the long cylindrical tube for testing under various flow rate (0~180 L/min), the solid line is the nonlinear best fit of original data (open circle) to modified king's model, y (volt) = 0.5197 V (flow rate)$^{0.2232}$, $R^2 = 0.95$.

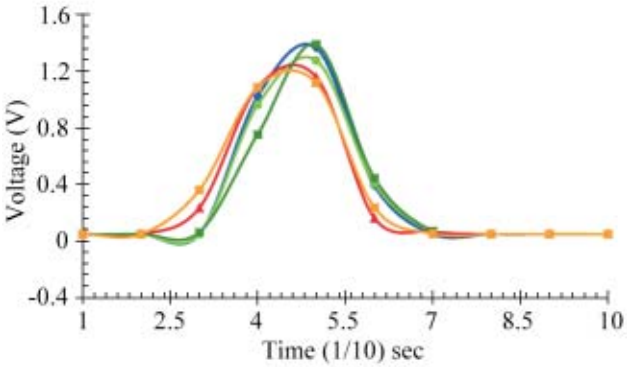

Figure 10. By using a 3 liter calibration syringe, five repetive measurements with area integral gives 2.981 ± 0.0081 liter. It is within the 3% acceptance criterion of ATS.

output of the analog circuit. The data is then nonlinear curve fitting by using Eq. (8). The resultant curve is then nonlinear cure fitting to find out the parameters. Figure 9 shows fitted result according to the modified King's law results in y (volt) = $0.5197*V^{0.2232}$, $R^2 = 0.9541$.

Figure 10 shows repetitive flow measurements by using a standard 3 liter syringe in the environmental control box with stable temperature (35 °C ~ 37 °C) and humidity (85 ~ 88%H). The area integral of resultant flow-time curves gives well repeatability. Five measurement results of area integral give average value of 2.981 with standard deviation of 0.0081 by a traceable flow meter. If the coverage factor = 2 and level of confidence = 95%, then we can obtain the expanded uncertainty is 0.096 liter (± 1.3%) for 3 liter syringe. The uncertainty of 3 liter volume test is less then ± 3%, which is within the recommended range by ATS.

4. Conclusions

A simple model for a micromachined thermal sensor was presented for the calculation of temperature distribution and conduction. Based on the simulation results, the heater geometry for each membrane size of the manufactured sensors is chosen around the optimum value for the sensor efficiency. The experimental results are in agreement with our design considerations. This was verified by measurements of the total power consumption in air at constant temperature. An increase in membrane size while keeping the heated membrane area constant led to reduced power consumption. In the future it is intended to integrate the operational amplifier analog circuit and processing electronics on the same chip or gas sensing film.

Acknowledgement

This project is supported in part by Ministry of Economic Affairs (Taiwan, R.O.C.). The assistance of ITRI-ERSO Allen Lin in flow analysis and Prof. A. B. Wang in thermal image analysis system is gratefully acknowledged.

References

[1] Centers for Disease Control and Prevention (CDC), *Morbidity and Mortality Weekly Report*, Vol. 47, pp. 1022–1025 (1998).

[2] U.S. Department of Health and Human Services, National Heart, Lung, and Blood Institute "Data Fact Sheet-Chronic Obstructive Pulmonary Disease (COPD)," May 2001.

[3] Anonymous, "Standardization of Spirometry, 1994 Update," *Am. J. Respir Crit Care Med*, Vol. 152, pp. 1107–1136 (1995).

[4] Van Putten, A. F. P. et al., "Multisensor Microsystem for Pulmonary Function Diagnostics," *IEEE Sensor Journal*, Vol. 2, No. 6 (2002).

[5] Chiu, J. P., "Micromachined Anemometer for Spirometric Application," N.T.U. Master Thesis, Taiwan, R.O.C. (1999).

[6] Chiu, N. F., "Development of MEMS Hot-Wire Chip for Portable Digital Electronic Spirometric System," N.T.U. Master Thesis, Taiwan, R.O.C. (2001).

[7] Jiang, F., Tai, Y. C., Ho, C. M., Karan, R., and Garstenauer, M., "Theoretical and Experimental Studies of Micromachined Hot-wire Anemometers," IEDM, IEEE, pp. 94–139, (1994).

[8] Udrea, F., Gardner, J. W., Setiadi, D., Covington, J. A., Dogaru, T., Lu, C. C. and Milne, W. I., "Design and Simulations of SOI CMOS Micro-hotplate Gas Sensor," *Sensors and Actuators B*, Vol. 78, pp. 180–190 (2001).

[9] Van Dijk, G. J. A. and Huijsing, J. H., "Bridge-output-to-frequency Converter for Smart Thermal air-flow Sensors," *IEEE Transactions on Instrumentation and Measurement*, Vol. 44, No. 4, (1995).

[10] Rasmussen, A. and Zaghloul, M. E., "In the Flow with MEMS," *IEEE Circuit & Device Journal* (1998).

[11] Bosch, R., "Micromachined Metal Oxide Gas Sensor Opportunities to Improve Sensor Performance," *Sensor and Actuators B*, Vol. 73, pp. 1–26 (2001).

[12] Bosch, R., "Micromachined Thermal Conductivity Hydrogen Detector for Automotive Applications," *IEEE*, pp. 1571–1575 (2002).

[13] Lin, C. W., Wang, D. H., Wang, H. C. and Wu, H. D., "Prototype Development of Digital Spirometer," *Proceedings of the 20th Annual International Conference of the IEEE Engineering in Medicine and Biology Society*, Vol. 20, No 4 (1998).

[14] Oliverira, A., Freire, R. C. S., Deep, G. S. and Lobo, P. C., "An Anemometer with PWM Exciation," *IEEE* (1995).

[15] King, L. V., , "On the Convection of Heat From Small Cylinders in a Stream of Fluid: Determination of the Convection Constants of Small Platinum Wires, with Applications to Hot-wire Anemometry," *Proc. R. Soc. London*, Vol. 90, pp. 563–570, in J. O. Hinze (1914).

Manuscript Received: Mar. 30, 2005
Accepted: Jul. 5, 2005